DOI: 10.19884/j.1672-5220.202502008

Dynamic Tracking Model for Spacecraft Center of Mass in Gravitational Wave Detection Based on IAROA-XGBoost

SUN Zihao[1], SHENG Xiaowei[1*], XU Yang[1], CAI Zhiming[2]
1. College of Mechanical Engineering, Donghua University, Shanghai 201620, China
2. Innovation Academy for Microsatellites of Chinese Academy of Sciences, Shanghai 201304, China

Abstract: During the in-orbit operation of gravitational wave detection spacecraft, the spacecraft center of mass (CoM) undergoes continuous changes due to various factors, which adversely affect detection accuracy. Existing CoM identification algorithms fail to meet real-time acquisition requirements and may disrupt the mission. To address this issue, a CoM dynamic tracking model is proposed, taking the rotation angles of the internal moving optical subassemblies (MOSA) and high-gain antenna (HGA) as input features and the spacecraft's CoM position coordinates as output variables. First, an improved attraction-repulsion optimization algorithm (IAROA) is developed to optimize the hyperparameters of the eXtreme Gradient Boosting (XGBoost) model, forming the IAROA-XGBoost model. Second, a discrete CoM-rotation angle mapping dataset is established by integrating a high-precision spacecraft finite element model with Latin hypercube sampling. Based on this dataset, a dynamic CoM tracking model is obtained by training with IAROA-XGBoost, and the accuracy of the model is compared with five commonly used machine learning models. Finally, SHapley Additive exPlanations (SHAP) is employed for interpretability analysis to identify the dominant factors influencing CoM position and investigate how feature interactions affect the model outputs. The results demonstrate that the proposed model achieves a CoM prediction accuracy better than 0.5 μm, outperforming the comparative models. It enables high-precision dynamic tracking of the spacecraft's CoM as it changes with component rotation angles, providing real-time and reliable CoM data for the spacecraft's Drag-Free Attitude and Control System, formation flight control, and CoM adjustment, ensuring the successful execution of the gravitational wave detection mission.

Keywords: gravitational wave detection; center of mass (CoM) prediction; attraction-repulsion optimization algorithm; eXtreme Gradient Boosting (XGBoost) model; SHapley Additive exPlanations (SHAP)
CLC number: V476 **Document code**: A
Article ID: 1672-5220(2026)05-0099-13

0 Introduction

Space-based gravitational wave detection opens a new observational window in the mid-to-low frequency range (0.1 mHz–1 Hz), offering significant insights into the origins and evolution of the universe, black hole mergers, dark matter, and dark energy[1-4]. In the "Taiji Program", three spacecraft in heliocentric orbits form a triangular formation with 3-million-kilometer arms. Each spacecraft carries two test masses (TMs) as inertial references. High-precision laser interferometry measures picometer-scale optical path variations between the TMs, enabling the retrieval of gravitational wave signals[5-6]. To achieve this precision, the spacecraft employ a Drag-Free Attitude and Control System (DFACS) to maintain the TMs in their central positions, isolating them from direct contact with the spacecraft. This setup protects the TMs from external non-conservative forces, such as solar radiation pressure, solar wind, and cosmic rays, ensuring that the TMs sustain an ultra-low residual acceleration noise level[7-9]. The spacecraft's center of mass (CoM) position, critical for DFACS and formation flight attitude and orbit control, deviates from its calibrated position during the in-orbit phase due to factors like propellant consumption, component configuration changes, and thermal deformations[10-11]. These deviations introduce additional rotational acceleration and gradient noise, and can lead to incorrect DFACS judgments, amplifying TM acceleration noise. In extreme cases, this may cause a collision between the TMs and the spacecraft[12-14]. Furthermore, CoM deviations can alter the formation's orbital and attitude states, disrupting laser link pointing between formation members and significantly affecting detection accuracy[15-16]. Thus, it is crucial to dynamically track CoM variations and obtain real-time position data to provide high-precision, continuous support for DFACS and formation flight attitude and orbit control systems.

Existing research on the in-orbit CoM variation of

Received date: 2025-02-14
Foundation item: National Key Research and Development Program of China (No. 2024YFC2207200)
* Correspondence should be addressed to SHENG Xiaowei, email: shengxw@dhu.edu.cn
Citation: Sun Z H, Sheng X W, Xu Y, et al. Dynamic tracking model for spacecraft center of mass in gravitational wave detection based on IAROA-XGBoost [J]. *Journal of Donghua University (English Edition)*, 2026, 43(5): 99-111.

spacecraft primarily focuses on CoM identification algorithms, with limited studies on CoM dynamic tracking. Wang et al.[17] proposed a high-precision and high-stability CoM identification method for spacecraft such as gravity satellites and gravitational wave detectors. This method utilizes periodic excitation signals with varying waveforms as system inputs via thrusters, and employs an Extended Kalman Filter (EKF) to identify the spacecraft's CoM. Simulation results show that, under triangular waveform excitation, the three-axis CoM identification error can be controlled within 4.46 μm. Wei et al.[18] addressed the in-orbit CoM identification problem for the Taiji-1 satellite by combining EKF and Rauch-Tung-Striebel smoothing to estimate CoM offsets. A chi-squared test was incorporated to eliminate outliers, and nonlinear least squares were used for cross-validation. The estimated accuracy achieved was 10 μm. Wang et al.[16], addressing the CoM variation issue for gravitational wave detectors, proposed a CoM identification method based on laser link constraints and incorporating Kalman filtering theory. Simulations were conducted to ensure the laser link alignment accuracy, with results indicating that this method achieved a CoM identification accuracy of 27 μm while maintaining the laser interferometer arm alignment precision better than 10 nanoradians.

In summary, while current in-orbit CoM identification algorithms can achieve high precision, they are limited by factors such as data update frequency, transmission delay, and computational speed, which prevent them from meeting the real-time CoM position retrieval requirements. Furthermore, most identification algorithms apply unidirectional torques via magnetorquers or thrusters. This approach leads to excessive spacecraft maneuvering angles and restricts the degrees of freedom during maneuvers, making it difficult to maintain the pointing accuracy of the inter-spacecraft laser link. Significant attitude deviations may severely disrupt the laser link and reduce the precision of gravitational wave detection. Meanwhile, the application of unidirectional torques inevitably alters the relative position between the spacecraft and the TM, introducing coupling disturbances between the spacecraft platform and the TM. The primary types of coupling disturbances include self-gravity, self-magnetic, and capacitive sensor interference. The magnitude of these coupling forces depends on the relative position and attitude between the spacecraft and the TM. Yue et al.[9] provided a detailed summary of the modeling methods for these disturbance forces and their associated noise. All of these disturbances negatively affect the maintenance of the TM's ultra-low residual acceleration noise level.

To address these issues, this study proposes three improvement strategies targeting the limitations of the attraction-repulsion optimization algorithm (AROA), including a good point set (GPS)-based population initialization method, an improved optimal individual attraction operator, and a nonlinear decreasing factor, aimed at enhancing the algorithm's optimization performance. Building upon this foundation, this study employs the improved AROA (IAROA) to optimize the hyperparameters of the eXtreme Gradient Boosting (XGBoost) model, and subsequently develops a CoM dynamic tracking model based on the IAROA-XGBoost framework. This model avoids reliance on driving torques and enables high-precision tracking and prediction of the spacecraft's CoM variations due to the rotation angles of the internal moving optical subassemblies (MOSA) and high-gain antenna (HGA), meeting real-time CoM retrieval needs for gravitational wave detection. Furthermore, the model is compared with five commonly used machine learning models on the same dataset, and SHapley Additive exPlanations (SHAP) theory is applied to interpret its outputs, improving interpretability and transparency.

1 IAROA-XGBoost

Gravitational wave detection missions impose extremely high precision requirements on CoM localization. Given the superior capability of XGBoost in handling nonlinear relationships and high-dimensional data, this study employs XGBoost to construct a CoM dynamic tracking model. Furthermore, an IAROA-based hyperparameter optimization strategy is proposed to optimize the XGBoost hyperparameters. This approach aims to balance model complexity and generalization ability, further improve model accuracy, and mitigate issues of overfitting and underfitting, thereby ensuring optimal performance on the CoM dataset and meeting the demands of the detection mission.

1.1 XGBoost

XGBoost is an improvement of the boosting algorithm based on gradient-boosted decision trees, utilizing Classification and Regression Trees (CART) as the base learners in an ensemble model[19-20]. Its principle is illustrated in Fig. 1, where v_1, v_2, v_3, and v_4 denote the leaf-node weights of individual CART-based trees. The expression is

$$\hat{y}_i = \sum_{k=1}^{t} f_k(\boldsymbol{x}_i),\ f_k \in F,\ i = 1, 2, \cdots, n, \quad (1)$$

where $\hat{y}_i$ is the predicted value for the ith sample; t denotes the total number of CART-based base learners contained in the ensemble model; k denotes the number of CART-based trees; F is the ensemble space of the CART-based trees; $\boldsymbol{x}_i$ is the feature vector of the ith sample; n denotes the total number of training samples.

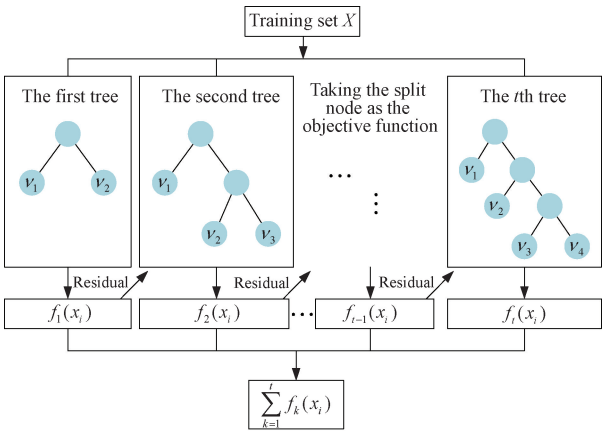


Fig. 1 Diagram of XGBoost principle

1.2 AROA and IAROA

AROA is a novel metaheuristic optimization algorithm proposed by Cymerys et al.[21] in 2024, which simulates attraction and repulsion phenomena in nature. The schematic of AROA is shown in Fig. 2. Each candidate individual is attracted by individuals with better fitness values and repelled by individuals with poorer fitness values, gradually moving toward the optimal individual throughout the optimization process.

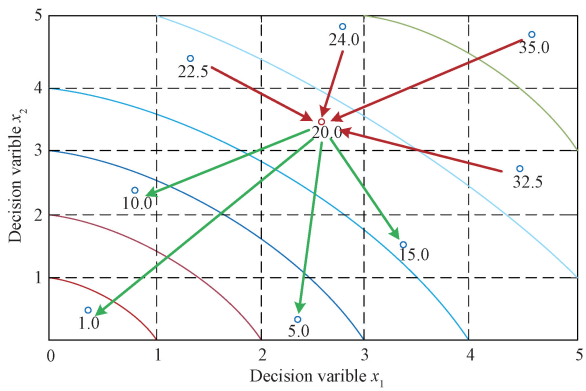


Fig. 2 Schematic of AROA

AROA determines the initial positions of the candidate individuals through random initialization:

$$\boldsymbol{X}_p = \text{rand}\,(\boldsymbol{X}_{\text{ub}} - \boldsymbol{X}_{\text{lb}}) + \boldsymbol{X}_{\text{lb}}, \tag{2}$$

where $\boldsymbol{X}_p$ is the initial position of the pth candidate individual; X_{lb} and X_{ub} are the lower and upper boundaries for each candidate individual, respectively.

AROA simulates the attraction and repulsion process between individuals using the attraction-repulsion operator $\boldsymbol{n}_p$, the optimal individual attraction operator $\boldsymbol{b}_p$, and the local search operator $\boldsymbol{s}_p$:

$$\boldsymbol{X}_p^{q+1} = \boldsymbol{X}_p^q + \boldsymbol{n}_p + \boldsymbol{b}_p + \boldsymbol{s}_p, \tag{3}$$

where $\boldsymbol{X}_p^q$ represents the position of the pth individual in the qth iteration, and the calculation formula for $\boldsymbol{n}_p$ is

$$\boldsymbol{n}_p = \frac{1}{N_n}\sum_{h=1}^{N_n} \gamma \cdot (\boldsymbol{X}_h - \boldsymbol{X}_p) \cdot H(d_{p,h}, d_{p,\max}) \cdot \varphi(f_h, f_p), \tag{4}$$

where γ is the step size coefficient; $d_{p,h}$ is the Euclidean distance between the pth individual and the hth individual; $d_{p,\max}$ denotes the maximum Euclidean distance between the pth individual and all neighboring individuals within its neighborhood; H is the function used to evaluate the influence of the hth individual; N_n is the number of individuals surrounding the current individual; $\varphi(f_h, f_p)$ is the function used to determine the update direction.

The calculation formula for $\boldsymbol{b}_p$ is

$$\boldsymbol{b}_p = \begin{cases} \gamma \cdot m \cdot (\boldsymbol{X}_{\text{best}}^q - \boldsymbol{X}_p^q), & r_1 \geqslant p_1, \\ \gamma \cdot m \cdot (\boldsymbol{a}_1 \cdot \boldsymbol{X}_{\text{best}}^q - \boldsymbol{X}_p^q), & r_1 < p_1, \end{cases} \tag{5}$$

where $\boldsymbol{X}_{\text{best}}^q$ is the optimal individual in the qth iteration; r_1 is a random number in the range of $[0, 1]$; p_1 is the probability threshold; $\boldsymbol{a}_1$ is a vector of random numbers in the range of $[0, 1]$; m is the balance factor.

The calculation formula for $\boldsymbol{s}_p$ is

$$\boldsymbol{s}_p = \begin{cases} \boldsymbol{s}_1, & r_3 > q/(2 \cdot Q_{\max}) + 0.25, \; r_2 < p_2, \\ \boldsymbol{s}_2, & r_3 \leqslant q/(2 \cdot Q_{\max}) + 0.25, \; r_2 < p_2, \\ \boldsymbol{s}_3, & r_2 \geqslant p_2, \end{cases} \tag{6}$$

where $Q_{\max}$ represents the maximum number of iterations; r_2 and r_3 are random numbers in the range of $[0, 1]$.

The calculation formulas for $\boldsymbol{s}_1$ to $\boldsymbol{s}_3$ are shown in Eqs. (7) to (9):

$$\boldsymbol{s}_1 = \boldsymbol{\mu}_1 \cdot N(0, \eta_1 \cdot \omega \cdot (\boldsymbol{X}_{\text{ub}} - \boldsymbol{X}_{\text{lb}})), \tag{7}$$

$$\boldsymbol{s}_2 = \begin{cases} \eta_2 \cdot \boldsymbol{\mu}_2 \cdot \omega \cdot \sin(2r_5\pi) \cdot |\boldsymbol{a}_2 \cdot \boldsymbol{X}_{\text{W}} - \boldsymbol{X}_p^q|, & r_4 < 0.5, \\ \eta_2 \cdot \boldsymbol{\mu}_2 \cdot \omega \cdot \cos(2r_5\pi) \cdot |\boldsymbol{a}_2 \cdot \boldsymbol{X}_{\text{W}} - \boldsymbol{X}_p^q|, & r_4 \geqslant 0.5, \end{cases} \tag{8}$$

$$\boldsymbol{s}_3 = \boldsymbol{\mu}_3 \cdot (2 \cdot \boldsymbol{a}_3 - \boldsymbol{L}) \cdot (\boldsymbol{X}_{\text{ub}} - \boldsymbol{X}_{\text{lb}}), \tag{9}$$

where r_4 and r_5 are random numbers in the range of $[0, 1]$; η_1 and η_2 are constants; $\boldsymbol{\mu}_1$, $\boldsymbol{\mu}_2$, and $\boldsymbol{\mu}_3$ are binary vectors with thresholds t_{r_1}, t_{r_2}, and t_{r_3}, respectively; $\boldsymbol{a}_2$ and $\boldsymbol{a}_3$ are vectors of random numbers in the range of $[0, 1]$; $\boldsymbol{X}_{\text{W}}$ is the individual selected through the roulette wheel strategy; ω is the linearly decreasing factor defined as $\omega = 1 - q/Q_{\max}$; $\boldsymbol{L}$ is the unit vector. After local search, AROA employs two population-based operators to influence all candidate individuals, and their calculation formulas are

$$\boldsymbol{X}_p^{q+1} = \begin{cases} \boldsymbol{X}_p^q + c_f \cdot (\boldsymbol{\mu}_4 \cdot (\boldsymbol{a}_4 \cdot (\boldsymbol{X}_{\text{ub}} - \boldsymbol{X}_{\text{lb}})) + \boldsymbol{X}_{\text{lb}}), & r_6 < e_f, \\ \boldsymbol{X}_p^q + (e_f \cdot (1 - r_7) + r_7)(\boldsymbol{X}_{r8}^q - \boldsymbol{X}_{r9}^q), & r_6 \geqslant e_f, \end{cases} \tag{10}$$

where $\boldsymbol{\mu}_4$ is a binary vector with a threshold of $1 - e_f$; e_f is the probability threshold; $\boldsymbol{a}_4$ is a vector of random numbers in the range of $[0, 1]$; r_6 and r_7 are random numbers in the range of $[0, 1]$; r_8 and r_9 are indices of randomly selected individuals; $c_f = (1 - q/Q_{\max})^3$.

Although AROA outperforms other metaheuristic algorithms in optimization performance, it still faces issues such as low-quality initial populations, a decline in population diversity in the later stages of iteration, and a

tendency to get stuck in local optima. To address these problems, three improvements are proposed to enhance the algorithm, resulting in an IAROA, as outlined below.

1) GPS initialization

The AROA determines the initial positions of candidate populations through random sampling, which may result in uneven distribution and fail to ensure consistent quality of the initial population across iterations. To address this limitation, a novel initialization methodology incorporating GPS has been developed[22-23], with the technical implementation described as follows.

Let G_D be the unit cube in D-dimensional Euclidean space. Suppose $r \in G_D$, and then the set of numbers in Eq. (11) can be called the GPS.

$$P_M(g)=\{(\{\rho_1^{(M)}g\},\{\rho_2^{(M)}g\},\cdots,\{\rho_D^{(M)}g\}) \mid g=1,2,\cdots,M\}, \tag{11}$$

where $P_M(g)$ denotes the GPS; M denotes the total number of good points; D denotes the dimensionality of the search space; ρ_D denotes the good point parameter, and $\rho_D=\{2\cos(2\pi d/p_r)\}$, $1\leqslant d\leqslant D$; p_r is taken as the smallest prime number of $(p_r-3)/2\geqslant D$. The deviation $\varphi(M)$ satisfies $\varphi(M)=C(\rho,\varepsilon)M^{-1+\varepsilon}$, where $C(\rho,\varepsilon)$ is a constant related only to $\varepsilon(\varepsilon>0)$. Then, $P_M(g)$ is mapped to the search space according to

$$\boldsymbol{X}_g(d)=(\boldsymbol{X}_{\mathrm{ub},d}-\boldsymbol{X}_{\mathrm{lb},d})\{\rho_d^{(M)}g\}+\boldsymbol{X}_{\mathrm{lb},d}, \tag{12}$$

To verify the effectiveness of GPS, cubic chaotic mapping and random initialization were compared. Assuming a population size of 500, a dimension of 1, and a range of [0, 1], the population distributions for the three initialization methods are shown in Fig. 3.

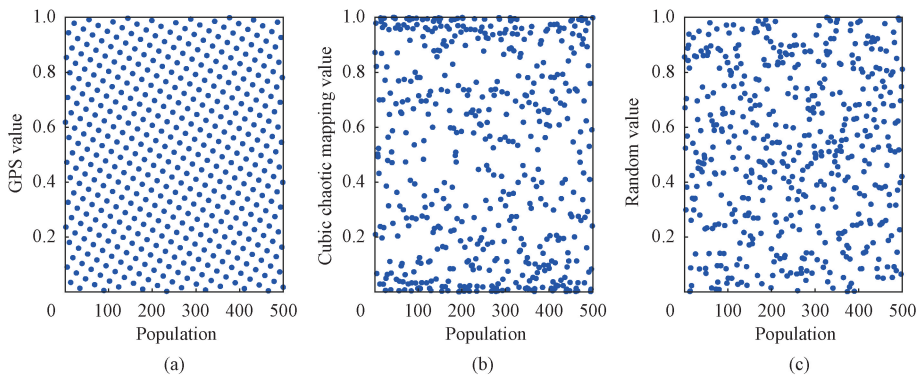


Fig. 3 Population distribution diagram of three initialization methods: (a) GPS initialization; (b) cubic chaotic mapping; (c) random initialization

Figure 3 reveals that the GPS initialization achieves superior spatial uniformity compared to cubic chaotic mapping and random initialization. This method demonstrates enhanced distribution stability without localized clustering or sparsity, ensuring consistent population initialization quality while establishing robust global search foundations for subsequent optimization processes.

2) Improved optimal individual attraction operator $\boldsymbol{b}'_p$

In $\boldsymbol{b}_p$, although a random vector $\boldsymbol{a}_1$ is introduced to prevent individuals from rapidly approaching the optimal individual, the approaching method is singular. This can exacerbate the reduction of population diversity in the later stages of iterations, causing the algorithm to fall into local optima. To address this limitation, $\boldsymbol{b}'_p$ has been developed, incorporating three distinct methods to progressively direct candidate individuals toward optimal individuals. This multi-modal method effectively mitigates population diversity loss during late iterations, with the specific implementation detailed below.

Method 1 Gradually approach the optimal individual in each dimension.

$$\boldsymbol{b}_1=\gamma\cdot m\cdot\boldsymbol{a}_4\cdot(\boldsymbol{X}^q_{\mathrm{best}}-\boldsymbol{X}^q_p). \tag{13}$$

Method 2 Simultaneously approach the optimal individual while avoiding the worst individual.

$$\boldsymbol{b}_2=\gamma\cdot m\cdot(\boldsymbol{a}_4\cdot(\boldsymbol{X}^q_{\mathrm{best}}-\boldsymbol{X}^q_p)-\boldsymbol{a}_5\cdot(\boldsymbol{X}^q_{\mathrm{worst}}-\boldsymbol{X}^q_p)). \tag{14}$$

Method 3 Utilize the gap between the optimal and worst individuals, and gradually achieve this gap in each dimension.

$$\boldsymbol{b}_3=\gamma\cdot m\cdot\boldsymbol{a}_4\cdot(\boldsymbol{X}^q_{\mathrm{best}}-\boldsymbol{X}^q_{\mathrm{worst}}), \tag{15}$$

where $\boldsymbol{X}^q_{\mathrm{worst}}$ is the worst individual in the qth iteration; $\boldsymbol{a}_4$ and $\boldsymbol{a}_5$ are vectors of random numbers in the range of [0, 1]. The schematic illustration of the three methods is shown in Fig. 4. These methods are assigned equal probabilities during the iteration process. Hence, $\boldsymbol{b}'_p$ is

$$\boldsymbol{b}'_p=\begin{cases}\boldsymbol{b}_1, & r_1\geqslant\dfrac{2}{3},\\ \boldsymbol{b}_2, & \dfrac{1}{3}\leqslant r_1<\dfrac{2}{3},\\ \boldsymbol{b}_3, & 0\leqslant r_1<\dfrac{1}{3},\end{cases} \tag{16}$$

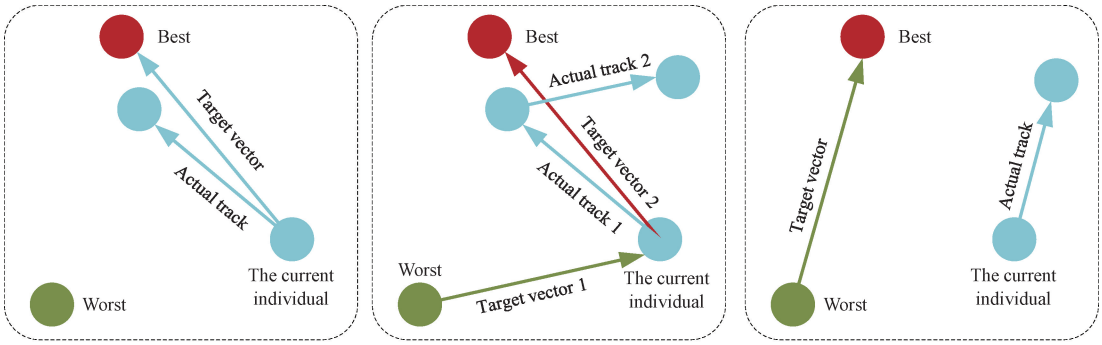


Fig. 4 Schematic diagram of three methods for approaching optimal individual: (a) method 1; (b) method 2; (c) method 3

3) Nonlinear decreasing factor ω'

In s_p, the linear decreasing factor ω controls both the degree of perturbation of s_1 and the follow-up distance of s_2. However, its linear decay characteristic is not conducive to balancing the AROA's global exploration and local exploitation capabilities. To address this issue, a nonlinear decreasing factor ω' is introduced. ω' maintains a low decay rate in the early iterations, preserving a relatively large value to enhance global exploration and prevent premature convergence. In the later iterations, its decay rate increases, leading to smaller values that reinforce local exploitation and enable precise optimal solution search.

$$\omega' = \begin{cases} 1 - \alpha \cdot \left(\dfrac{1}{\alpha} \cdot \dfrac{q}{Q_{\max}} \right)^{\beta}, & 0 \leqslant \dfrac{q}{Q_{\max}} \leqslant \alpha, \\ (1-\alpha) \cdot \left(\left(1 - \dfrac{q}{Q_{\max}} \right) \cdot \dfrac{1}{1-\alpha} \right)^{\beta}, & \alpha < \dfrac{q}{Q_{\max}} \leqslant 1, \end{cases} \tag{17}$$

where α and β are adjustment factors. α controls the inflection point of the decay rate change in ω', and β determines the overall decay rate magnitude. When $\beta = 3.0$, the iteration curves of ω' under different values of α are shown in Fig. 5(a); when $\alpha = 0.7$, the iteration curves of ω' under different values of β are illustrated in Fig. 5(b).

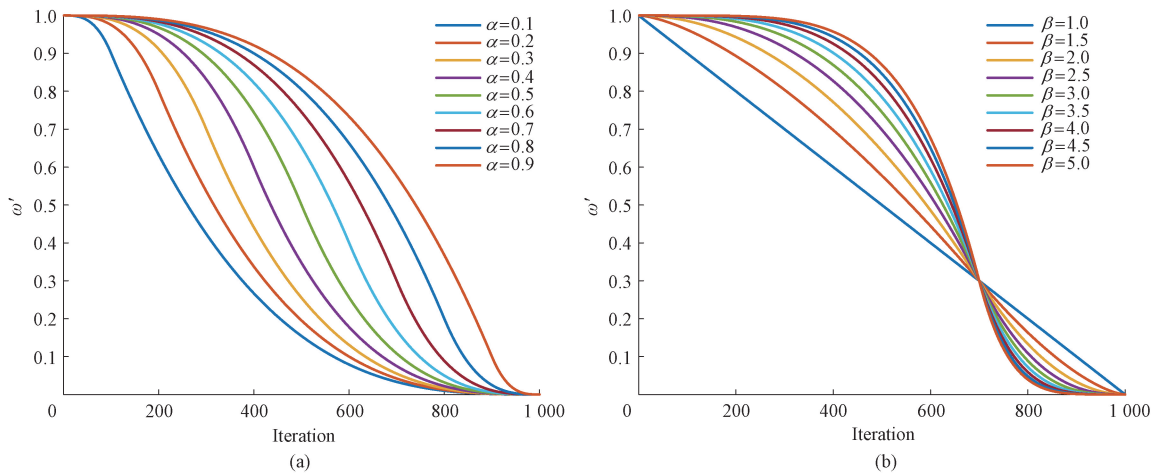


Fig. 5 Iteration curves of ω': (a) under different values of α with $\beta = 3.0$; (b) under different values of β with $\alpha = 0.7$

1.3 Hyperparameter optimization

The primary hyperparameters of XGBoost include the number of regression trees (n_estimators), maximum tree depth (max_depth), learning rate (eta), subsample ratio (subsample), column subsample ratio (colsample_bytree), minimum child weight (min_child_weight), and minimum loss reduction (gamma). The definition and impact of each hyperparameter on the model is summarized in Table 1.

Table 1 Definitions and impacts of XGBoost hyperparameters

Hyperparameter	Definition & role	Impact of low value	Impact of high value
n_estimators	Number of regression trees; controls model fit and generalization ability	Underfitting; high prediction bias	Overfitting; increased complexity and training time
max_depth	Controls complexity of features captured by each tree	Model too simple; poor feature capture	Overfitting
eta	Contribution of each tree to the final prediction	Stable but slow training; more trees needed	Fast convergence; prone to overfitting
subsample	Ratio of samples used per training iteration	Potential loss of critical information	Reduced generalization capability
colsample_bytree	Ratio of features selected randomly per tree	Ignoring critical features	Increased redundancy; reduced generalization
min_child_weight	Minimum sum of sample weights required for leaf splits	Risk of overfitting, capturing noise	Overly conservative model; weakened local feature capture
gamma	Minimum loss reduction required for further splits	Excessive splits causing overfitting	Overly simple model; insufficient complexity for data fitting

As shown in Table 1, the values of XGBoost hyperparameters have a significant impact on the model's prediction accuracy and generalization capability. Since default hyperparameter settings often fail to accommodate the specific characteristics of different datasets, they may result in underfitting or overfitting. Therefore, this study employs the IAROA to optimize the hyperparameters of XGBoost to minimize the root-mean-square error (RMSE) between the predicted and actual values. The performance of each hyperparameter combination is evaluated using N_{cv}-fold cross-validation, where N_{cv} denotes the number of folds used in cross-validation. The overall process is illustrated in Fig. 6.

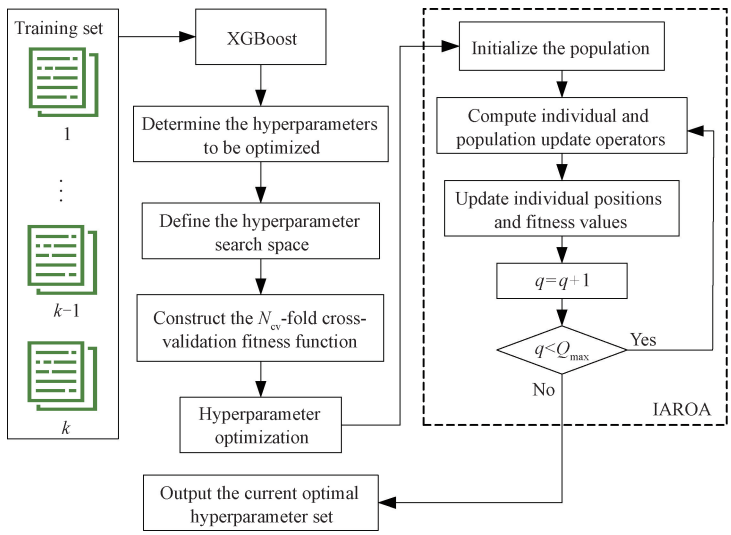


Fig. 6 Flowchart of XGBoost hyperparameter optimization

2 Construction of CoM Dynamic Tracking Model

2.1 Determination of input features and output variables

MOSA, as the payload of the gravitational wave detection spacecraft, consists of two core measurement systems (CMSs), each comprising a telescope system, an interferometer platform, and an inertial sensor housing the TM. During the mission, the angles of the CMSs are continuously adjusted to ensure high-precision laser interferometric measurements. The HGA, a key component for space-to-ground data transmission, relies on X-axis and Y-axis drive mechanisms for dual-axis rotation to maintain stable and continuous communication throughout the mission. The structural schematic of both components is shown in Fig. 7.

The continuous variation in the rotation angles of the MOSA and the HGA exerts a persistent influence on the spacecraft's CoM. Therefore, the MOSA rotation angles θ_1 and θ_2, along with the HGA rotation angles φ_1 and φ_2, are selected as input features for the CoM dynamic tracking model, while the spacecraft's CoM position coordinates serve as output variables. To facilitate the description of the deviation between the actual and designed CoM positions, a spacecraft body coordinate system O_{SC}-$X_{SC}Y_{SC}Z_{SC}$ is established. The origin O_{SC} is set at the designed CoM position, defined as the midpoint of the geometric centerline connecting the two TMs when both the telescopes and TMs are in their nominal positions. The X_{SC}-axis lies parallel to the spacecraft-launch vehicle separation plane, aligned with the symmetry axis of the two telescopes in their nominal 60° configuration and pointing in the direction of the telescope tubes. The Z_{SC}-axis is perpendicular to the separation plane, directed from the launch vehicle toward the spacecraft. The Y_{SC}-axis is determined following the right-hand rule, ensuring orthogonality with both the X_{SC}-axis and Z_{SC}-axis.

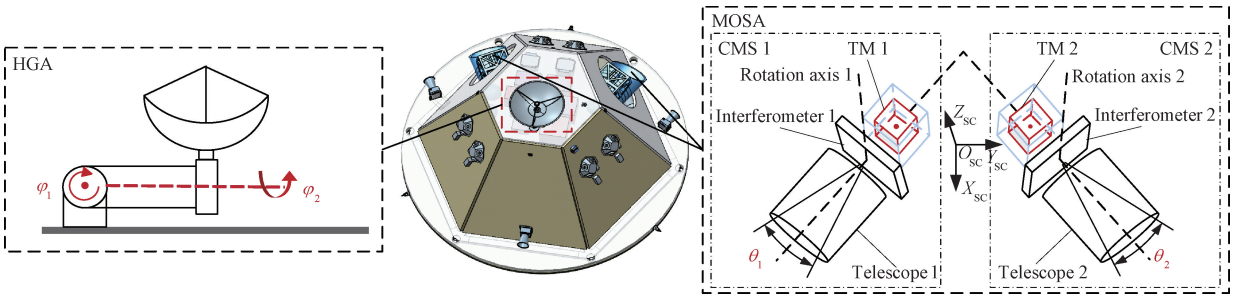


Fig. 7 Schematic diagram of HGA and MOSA structure

2.2 Construction of CoM-rotation angle discrete mapping dataset

After defining the inputs and outputs of the CoM dynamic tracking model, an appropriate sampling method must be selected to generate uniformly distributed sample points within the input feature space. Since the input features include the rotation angles of the MOSA and the HGA, dataset construction falls under the category of multidimensional sampling. To ensure uniformity and comprehensiveness, Latin Hypercube Sampling (LHS) is employed to generate input samples. LHS is a stratified sampling technique that approximates random sampling from a multidimensional parameter distribution. The LHS process is illustrated in Fig. 8.

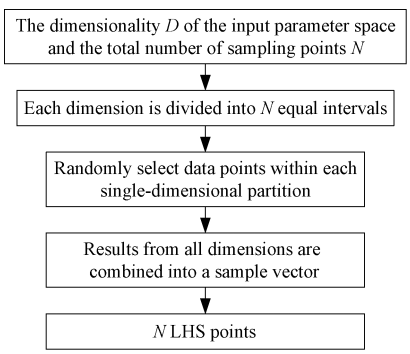


Fig. 8 Schematic diagram of LHS process

LHS offers excellent spatial coverage, mitigates clustering effects, and enhances the uniformity and global representativeness of sample point distribution[24-25].

After obtaining the input samples, it is necessary to accurately compute the corresponding output variables in order to construct a complete CoM-rotation angle discrete mapping dataset. A finite element-based centroid calculation method is employed, in which the spacecraft's three-dimensional (3D) structural model is discretized into a finite element model. The CoM coordinates and mass information of each mesh element are extracted, and the spacecraft's CoM position for each sample point is computed by

$$\boldsymbol{r}_c = \frac{\sum_{e=1}^{N_e} m_e \boldsymbol{r}_e}{\sum_{e=1}^{N_e} m_e}, \tag{18}$$

where $\boldsymbol{r}_c$ is the vector of the CoM relative to the coordinate system origin; $\boldsymbol{r}_e$ is the vector of the CoM of the eth mesh with respect to the origin of the coordinate system; m_e is the mass of the eth mesh; N_e is the total number of meshes.

The CoM coordinates and mass parameters of the MOSA, the HGA, and the spacecraft, when all assemblies are positioned at their nominal locations, are calculated based on the data derived from the spacecraft finite element model and are shown in Table 2.

Table 2 CoM coordinates and mass parameters for spacecraft and their components

Component	CoM coordinate/mm			Mass/kg
	X-axis	*Y*-axis	*Z*-axis	
MOSA	223.148 625 224 04	8.308 502 271 876 8	14.227 986 151 854	83.473 896 337 485 1
HGA	−117.580 661 538 01	−1.750 535 435 031 7	−773.792 949 304 160	12.512 497 575 934 9
Spacecraft	−115.758 760 708 42	22.430 987 073 023 0	48.546 086 448 818	670.484 328 980 626 7

2.3 Dataset preprocessing

Due to the dimensional differences between input features, directly using the dataset for training may affect the learning performance and stability of the CoM dynamic tracking model. Therefore, the min-max normalization method is applied to map the dataset to the range of $[0,1]$, as expressed as

$$z_{\text{norm}} = \frac{z - z_{\min}}{z_{\max} - z_{\min}}, \tag{19}$$

where z_{norm} is the normalized data; z is the data before normalization; $z_{\min}$ is the minimum value of the data; $z_{\max}$ is the maximum value of the data.

The normalized dataset will be randomly divided into a training set and a test set, with 80% allocated for training and 20% for testing. This division helps evaluate the model's performance on an independent dataset, validates its generalization ability, and prevents overfitting.

2.4 Model training and result analysis

The normalized dataset is fed into the IAROA-XGBoost model for hyperparameter optimization, and the optimal hyperparameter combination obtained is shown in Table 3.

Table 3 Optimal hyperparameter combination for IAROA-XGBoost

n_estimators	max_depth	eta	subsample	colsample_bytree	min_child_weight	gamma
1 614	3	0.086 16	0.918 956	0.847 866	10	0.346 871

Based on the optimal hyperparameter combination, the CoM dynamic tracking model is established. The model's accuracy and generalization capability are evaluated using mean absolute error E_{MA}, root mean square error E_{RM}, mean absolute percentage error E_{MP}, and goodness of fit E_{GF}. The formulas for each metric are

$$E_{\text{MA}} = \frac{1}{n_s}\sum_{s=1}^{n_s} |\hat{y}_s - y_s|, \tag{20}$$

$$E_{\text{RM}} = \sqrt{\frac{1}{n_s}\sum_{s=1}^{n_s} (\hat{y}_s - y_s)^2}, \tag{21}$$

$$E_{\text{MP}} = \frac{1}{n_s}\sum_{s=1}^{n_s} \frac{|y_s - \hat{y}_s|}{|y_s|} \times 100\%, \tag{22}$$

$$E_{\text{GF}} = 1 - \frac{\sum_{s=1}^{n_s} (y_s - \bar{y})(\hat{y}_s - \bar{y}')}{\sqrt{\sum_{s=1}^{n_s} (y_s - \bar{y})^2}\sqrt{\sum_{s=1}^{n_s} (\hat{y}_s - \bar{y}')^2}}, \tag{23}$$

where n_s is the total number of samples; y_s is the true value; $\hat{y}_s$ is the predicted value; $\bar{y}$ is the average true value; $\bar{y}'$ is the average predicted value.

The analysis results are presented in Table 4.

Table 4 Prediction performance of CoM dynamic tracking model

Sample set	Evaluation metric	Prediction error			
		X-axis	*Y*-axis	*Z*-axis	Overall
Training set	E_{MA}	2.475×10^{-4}	2.481×10^{-4}	2.491×10^{-4}	2.483×10^{-4}
	E_{RM}	2.866×10^{-4}	2.871×10^{-4}	2.881×10^{-4}	2.872×10^{-4}
	E_{MP}	0.001 160%	0.001 111%	0.000 473%	0.000 915%
	E_{GF}	1.139×10^{-7}	4.626×10^{-7}	5.718×10^{-8}	2.112×10^{-7}
Test set	E_{MA}	2.480×10^{-4}	2.495×10^{-4}	2.513×10^{-4}	2.497×10^{-4}
	E_{RM}	2.876×10^{-4}	2.884×10^{-4}	2.907×10^{-4}	2.889×10^{-4}
	E_{MP}	0.001 184%	0.001 117%	0.000 477%	0.000 926%
	E_{GF}	1.154×10^{-7}	4.662×10^{-7}	5.834×10^{-8}	2.133×10^{-7}
Full dataset	E_{MA}	2.477×10^{-4}	2.484×10^{-4}	2.496×10^{-4}	2.486×10^{-4}
	E_{RM}	2.868×10^{-4}	2.873×10^{-4}	2.886×10^{-4}	2.876×10^{-4}
	E_{MP}	0.001 165%	0.001 112%	0.000 474%	0.000 917%
	E_{GF}	1.142×10^{-7}	4.633×10^{-7}	5.741×10^{-8}	2.117×10^{-7}

According to Table 4 and the definition of E_{MA}, the model's average prediction errors for the CoM coordinates along the X, Y, and Z axes on the full dataset are 2.477×10^{-4}, 2.484×10^{-4}, and 2.496×10^{-4}, respectively. Consequently, the overall CoM prediction error is calculated as

$$\delta_C = \sqrt{\delta_X^2 + \delta_Y^2 + \delta_Z^2}, \tag{24}$$

where δ_C is the mean prediction error of the spacecraft's CoM; δ_X is the mean prediction error of the spacecraft's CoM X-axis coordinate; δ_Y is the mean prediction error of the spacecraft's CoM Y-axis coordinate; δ_Z is the mean prediction error of the spacecraft's CoM Z-axis coordinate. The resultant overall error on the full dataset is 4.177×10^{-4}.

The results demonstrate that the proposed model exhibits outstanding prediction accuracy and generalization capability, fully meeting the precision requirements for CoM localization in gravitational wave detection missions. To further validate the model's overall performance and the effectiveness of hyperparameter optimization, a comparative analysis was conducted against basic XGBoost and other state-of-the-art machine learning models on the same dataset. The results are summarized in Table 5.

Table 5 Comparison of machine learning results

Model	Evaluation metric	Prediction error			
		X-axis	Y-axis	Z-axis	Overall
Support vector regression (SVR)	E_{MA}	2.108×10^{-1}	4.132×10^{-2}	2.652×10^{-1}	1.724×10^{-1}
	E_{RM}	2.202×10^{-1}	5.644×10^{-2}	2.791×10^{-1}	2.078×10^{-1}
	E_{MP}	0.183 769%	0.185 058%	0.502 875%	0.290 568%
	E_{GF}	6.732×10^{-2}	1.787×10^{-2}	5.366×10^{-2}	4.629×10^{-2}
BP neural network	E_{MA}	1.663×10^{-2}	4.333×10^{-3}	1.425×10^{-2}	1.174×10^{-2}
	E_{RM}	2.074×10^{-2}	5.823×10^{-3}	1.824×10^{-2}	1.629×10^{-2}
	E_{MP}	0.014 511%	0.019 375%	0.027 026%	0.020 304%
	E_{GF}	5.973×10^{-4}	1.902×10^{-4}	2.293×10^{-4}	3.389×10^{-4}
Polynomial fitting	E_{MA}	5.372×10^{-3}	2.015×10^{-3}	4.242×10^{-3}	3.876×10^{-3}
	E_{RM}	7.088×10^{-3}	2.549×10^{-3}	5.394×10^{-3}	5.349×10^{-3}
	E_{MP}	0.004 701%	0.009 021%	0.008 116%	0.007 279%
	E_{GF}	6.975×10^{-5}	3.648×10^{-5}	2.005×10^{-5}	4.209×10^{-5}
LightGBM	E_{MA}	4.474×10^{-3}	2.219×10^{-3}	3.897×10^{-3}	3.530×10^{-3}
	E_{RM}	5.795×10^{-3}	2.831×10^{-3}	4.984×10^{-3}	4.706×10^{-3}
	E_{MP}	0.003 910%	0.009 937%	0.007 454%	0.007 101%
	E_{GF}	4.663×10^{-5}	4.496×10^{-5}	1.712×10^{-5}	3.624×10^{-5}
XGBoost	E_{MA}	3.239×10^{-2}	6.103×10^{-3}	3.039×10^{-2}	2.296×10^{-2}
	E_{RM}	4.318×10^{-2}	8.168×10^{-3}	3.940×10^{-2}	3.408×10^{-2}
	E_{MP}	0.028 325%	0.027 329%	0.057 994%	0.037 883%
	E_{GF}	2.589×10^{-3}	3.743×10^{-4}	1.069×10^{-3}	1.344×10^{-3}
IAROA-XGBoost	E_{MA}	2.477×10^{-4}	2.484×10^{-4}	2.496×10^{-4}	2.486×10^{-4}
	E_{RM}	2.868×10^{-4}	2.873×10^{-4}	2.886×10^{-4}	2.876×10^{-4}
	E_{MP}	0.001 165%	0.001 112%	0.000 474%	0.000 917%
	E_{GF}	1.142×10^{-7}	4.633×10^{-7}	5.741×10^{-8}	2.117×10^{-7}

Table 5 shows that the CoM dynamic tracking model trained using IAROA-XGBoost outperforms the other five models in terms of all evaluation metrics, achieving substantial improvements. This result fully demonstrates the effectiveness of the IAROA-based hyperparameter optimisation process in improving the overall performance of XGBoost, as well as the superiority of IAROA-XGBoost over traditional machine learning models in terms of prediction accuracy and generalization ability. This ensures optimal overall performance on the current dataset and enables better adaptation to the requirements of the gravitational wave detection task.

3 Interpretability Analysis of CoM Dynamic Tracking Model

Although the CoM dynamic tracking model exhibits excellent predictive performance, the inherent complexity of machine learning algorithms often renders them "black boxes" with limited interpretability. SHAP, based on the Shapley value theory in game theory, quantifies the

contribution of each input feature to the model output, providing a clear and systematic approach for analyzing the model's predictive logic and feature importance[26-27]. Therefore, SHAP is employed to interpret the model by analyzing summary plots of various features, identifying the dominant factors influencing the spacecraft's CoM position, elucidating the impact of different features on the model's predictions, and further examining the interaction effects among specific features. This enhances the model's interpretability and transparency.

3.1 SHAP feature summary analysis

SHAP quantifies the overall impact of each input feature on the model output by calculating the mean absolute SHAP values across all samples. The analysis results are shown in Fig. 9.

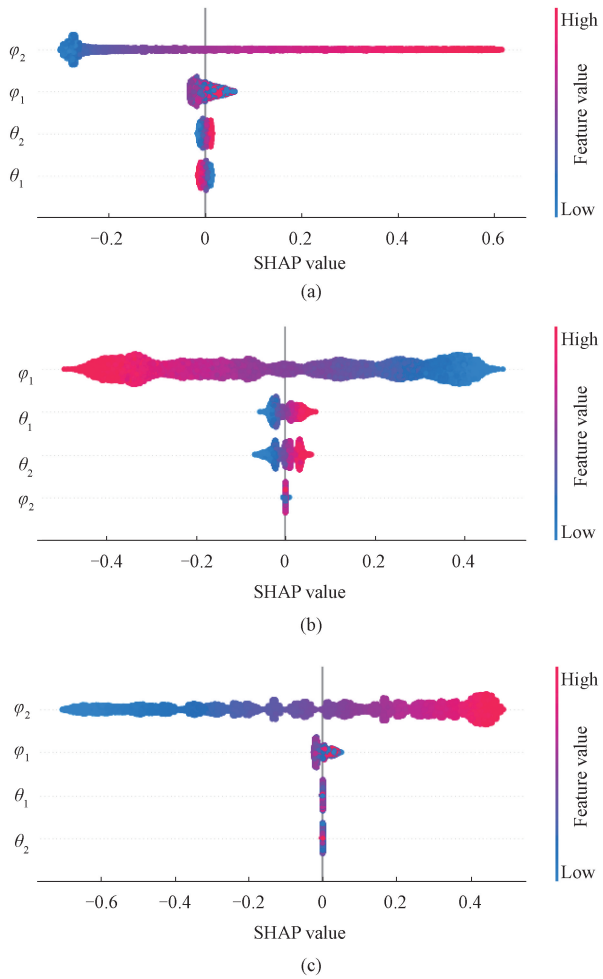


Fig. 9 Summary plots for each output variable: (a) CoM *X*-axis coordinate; (b) CoM *Y*-axis coordinate; (c) CoM *Z*-axis coordinate

In Fig. 9, different rows represent different features, with colors indicating the magnitude of the feature values (red for high, blue for low). The horizontal axis corresponds to the SHAP values of the features, which represent the weight of their influence on the prediction. A SHAP value greater than 0 indicates a positive impact on the prediction result, while a SHAP value less than 0 indicates a negative impact. On the vertical axis, the features are ranked by their importance, with those at the top having a greater influence on the model's output. The density of overlapping points reflects the distribution of SHAP values. Since the rotational angles θ_1 and θ_2 of the MOSA have a smaller range of variation, their impact on the prediction of the spacecraft's CoM coordinates is not significant. The rotational angle φ_2 of the HGA has a dominant influence on the prediction of the CoM *X*-axis and *Z*-axis coordinates, and the relationship is positive. For the CoM *Y*-axis coordinate prediction, the SHAP values of φ_2 are concentrated near 0, indicating its minor impact on the prediction. In contrast, for the CoM *Y*-axis output, the SHAP value distribution of φ_1 is the widest, and its impact on the prediction is most significant, showing a negative correlation.

The SHAP summary analysis clarifies both the magnitude and direction of the influence that the rotation angles of the MOSA and the HGA exert on the spacecraft's CoM. This insight can be utilized to develop a rational rotation strategy for the HGA, ensuring that angular changes under different operational modes do not result in excessive CoM shifts. At the same time, with the in-depth analysis of the influence of each component's rotation on the spacecraft's CoM position, the compensation strategy of the spacecraft's internal CoM adjustment mechanism can be further optimized to achieve the maximum degree of compensation during the rotation of the components, and thus improve the stability of the spacecraft's on-orbit operation attitude and control accuracy.

3.2 Feature interaction influence analysis

Among the model input features, there exists an interactive relationship between the HGA rotation angles φ_1 and φ_2. Therefore, taking the prediction of the CoM *Z*-axis coordinate as an example, the SHAP feature interaction plot is adopted to analyze the impact of the interaction between these two features on the model output. The analysis results are shown in Fig. 10.

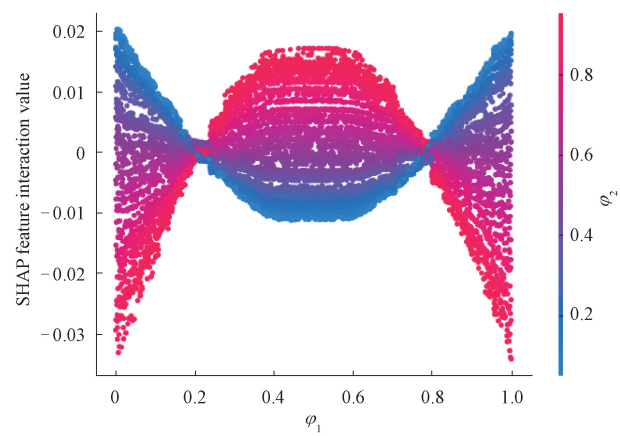


Fig. 10 SHAP feature interaction plot for HGA rotation angles

As shown in Fig. 10, the combined effect of the two rotation angles of the HGA, φ_1 and φ_2, on the spacecraft's CoM exhibits pronounced nonlinearity and symmetry. When φ_1 approaches the extreme values of its rotational range and φ_2 is also near its respective limits, the impact on the CoM is significantly amplified. In contrast, when φ_1 is within the mid-range region, the SHAP feature interaction values corresponding to different φ_2 settings become more concentrated. This indicates that under these conditions, variations in the HGA rotational angle have a relatively moderate effect on the spacecraft's CoM.

Overall, the interaction analysis of φ_1 and φ_2 indicates that their combined influence on the spacecraft's CoM exhibits strong coupling in both magnitude and direction, with a clear dependence on specific angular regions. Simultaneous large adjustments of both φ_1 and φ_2 will lead to more significant shifts in the CoM, which could introduce greater disturbances to the attitude and orbit control system. Therefore, when designing the HGA rotation strategy, the coupling effect between φ_1 and φ_2 should be fully considered. On one hand, it is advisable to avoid placing both angles at extreme values simultaneously to minimize disturbances to the spacecraft's CoM. On the other hand, when large and rapid adjustments are required, the model's predictions can be used to pre-evaluate the expected CoM shift and its impact on control torque. This enables adjustments to the attitude control algorithm or increases in control margins to ensure the stability of the spacecraft's attitude and orbit.

4 Conclusions

This study develops an IAROA-XGBoost model for dynamic spacecraft CoM tracking using MOSA and HGA rotation angles as input features. IAROA improves population initialization, population diversity, and the exploration-exploitation balance, enabling effective hyperparameter optimization of XGBoost. Based on the LHS-finite-element CoM-rotation-angle mapping dataset, the IAROA-XGBoost model achieves a CoM prediction accuracy better than 0.5 μm and an E_{GF} of 2.117×10^{-7}, outperforming the comparative machine learning models. SHAP analysis identifies φ_2 as the dominant feature for *X*-axis and *Z*-axis CoM predictions and φ_1 as the dominant feature for the *Y*-axis prediction, with significant interaction effects between φ_1 and φ_2. The proposed model enables real-time CoM position prediction without using driving torque as an input, providing an effective approach for dynamic CoM tracking of gravitational-wave detection spacecraft.

References

[1] Riles K. Gravitational waves: sources, detectors and searches [J]. *Progress in Particle and Nuclear Physics*, 2013, 68: 1-54.

[2] Mastrogiovanni S, Karathanasis C, Gair J, et al. Cosmology with gravitational waves: a review [J]. *Annalen der Physik*, 2024, 536(2): 2200180.

[3] Giammarchi M, Ricci F. Gravitational waves, event horizons and black hole observation: a new frontier in fundamental physics [J]. *Symmetry*, 2022, 14(11): 2276.

[4] Ni W T. Space gravitational wave detection: progress and outlook [J]. *Scientia Sinica (Physica, Mechanica & Astronomica)*, 2024, 54(7): 270402.

[5] Hu W R, Wu Y L. The Taiji Program in Space for gravitational wave physics and the nature of gravity [J]. *National Science Review*, 2017, 4(5): 685-686.

[6] Luo Z R, Wang Y, Wu Y L, et al. The Taiji program: a concise overview [J]. *Progress of Theoretical and Experimental Physics*, 2021, 2021(5): 05A108.

[7] Luo Z R, Zhang M, Jin G, et al. Introduction of Chinese space-borne gravitational wave detection program "Taiji" and "Taiji-1" satellite mission [J]. *Journal of Deep Space Exploration*, 2020, 7(1): 3-10.

[8] Jiao B H, Liu Q F, Dang Z H, et al. A review on DFACS (Ⅰ): system design and dynamics modeling [J]. *Chinese Journal of Aeronautics*, 2024, 37(5): 92-119.

[9] Yue C L, Jiao B H, Dang Z H, et al. A review on DFACS (Ⅱ): modeling and analysis of disturbances and noises [J]. *Chinese Journal of Aeronautics*, 2024, 37(5): 120-147.

[10] Hartig M S, Wanner G. Tilt-to-length coupling in LISA Pathfinder: analytical modeling [J]. *Physical Review D*, 2023, 108(2): 022008.

[11] Bassan M, Cavalleri A, De Laurentis M, et al. Actuation crosstalk in free-falling systems: torsion pendulum results for the engineering model of the LISA Pathfinder gravitational reference sensor [J]. *Astroparticle Physics*, 2018, 97: 19-26.

[12] Luo Z R, Bai S, Bian X, et al. Gravitational wave detection by space laser interferometry [J]. *Advances in Mechanics*, 2013, 43(4): 415-447.

[13] Park I H. Detection of low-frequency gravitational waves [J]. *Journal of the Korean*

Physical Society, 2021, 78(10): 886-891.

[14] Kawamura S, Ando M, Seto N, et al. Current status of space gravitational wave antenna DECIGO and B-DECIGO [J]. *Progress of Theoretical and Experimental Physics*, 2021, 2021(5): 05A105.

[15] Armano M, Audley H, Baird J, et al. Calibrating the system dynamics of LISA Pathfinder [J]. *Physical Review D*, 2018, 97(12): 122002.

[16] Wang S N, Zhang H B, Cai L, et al. Research on mass center identification for gravitational wave detection spacecraft with guaranteed laser link pointing accuracy [J]. *Remote Sensing*, 2025, 17(2): 296.

[17] Wang Z M, Li M, Zhao H C, et al. Research on a high-precision and high-stability method for identifying the spacecraft center of mass position based on periodic excitation signals [C]//The 15th National Conference on Vibration Theory and Application (NVTA2023). Nanjing: Chinese Society for Vibration Engineering (CSVE), 2023: 242. (in Chinese)

[18] Wei X T, Huang L, Shen T Y, et al. Calibration of the in-orbit center-of-mass of Taiji-1 [J]. *Physical Review D*, 2023, 108(8): 082001.

[19] Chen T Q, Guestrin C. XGBoost: a scalable tree boosting system [C]//22nd ACM SIGKDD International Conference on Knowledge Discovery and Data Mining. New York: ACM, 2016: 785-794.

[20] Qiu Y G, Zhou J, Khandelwal M, et al. Performance evaluation of hybrid WOA-XGBoost, GWO-XGBoost and BO-XGBoost models to predict blast-induced ground vibration [J]. *Engineering with Computers*, 2022, 38(5): 4145-4162.

[21] Cymerys K, Oszust M. Attraction-repulsion optimization algorithm for global optimization problems [J]. *Swarm and Evolutionary Computation*, 2024, 84: 101459.

[22] Guo Q, Li Y, Yang D. Convergence analysis and application of an improved sparrow search algorithm[J]. *Control and Decision*, 2024, 39(5): 1-9. (in Chinese)

[23] Li J, Ni Z, Zhu X H, et al. Drought prediction model based on GPSGSO-BPNN parallel ensemble learning algorithm [J]. *Systems Engineering: Theory and Practice*, 2018, 38(5): 1343-1353. (in Chinese)

[24] Mckay M D, Beckman R J, Conover W J. A comparison of three methods for selecting values of input variables in the analysis of output from a computer code [J]. *Technometrics*, 2000, 42(1): 55-61.

[25] Roshanian J, Ebrahimi M. Latin hypercube sampling applied to reliability-based multidisciplinary design optimization of a launch vehicle[J]. *Aerospace Science and Technology*, 2013, 28(1): 297-304.

[26] Mangalathu S, Hwang S H, Jeon J S. Failure mode and effects analysis of RC members based on machine-learning-based SHapley Additive exPlanations (SHAP) approach[J]. *Engineering Structures*, 2020, 219: 110927.

[27] Wu Y Q, Zhou Y S. Hybrid machine learning model and Shapley Additive exPlanations for compressive strength of sustainable concrete[J]. *Construction and Building Materials*, 2022, 330: 127298.

基于 IAROA-XGBoost 的引力波探测航天器质心动态跟踪模型构建

孙子昊[1]，盛晓伟[1*]，徐　洋[1]，蔡志鸣[2]

1. 东华大学 机械工程学院，上海 201620

2. 中国科学院微小卫星创新研究院，上海 201304

摘　要：引力波探测航天器在轨运行期间，其质心因受多种因素的影响会持续变化，继而影响探测精度。现有的在轨质心辨识算法无法满足实时获取质心位置的需求，并且辨识过程可能会对探测任务产生干扰。针对该问题，本文以引力波探测航天器在轨运行阶段中的舱内移动光学组件和高增益天线转动角度为输入特征，以航天器质心位置坐标为输出变量，建立了一种质心动态跟踪模型。首先，提出改进的吸引−排斥优化算法(improved attraction-repulsion optimization algorithm，IAROA)优化极端梯度提升(eXtreme Gradient Boosting，XGBoost)模型超参数组合，形成 IAROA-XGBoost 模型。其次，结合高精度航天器有限元模型与拉丁超立方采样建立了质心−转动角度的离散映射数据集；基于该数据集，采用 IAROA-XGBoost 训练得到了质心动态跟踪模型，并和 5 种常用的机器学习模型进行了精度对比。最后，引入沙普利加性解释对模型进行了可解释性分析，定位了质心位置的主导性影响因素，并分析了特征之间的交互作用对模型输出的影响。结果表明，该模型质心预测精度优于 0.5 μm，性能优于对比模型。该模型可实现航天器质心随构件转动角度变化的高精度动态跟踪预测，为引力波探测航天器无拖曳控制、探测编队姿轨控制及质心调整提供实时可靠的质心数据，保障引力波探测任务的顺利开展。

关键词：引力波探测；质心预测；吸引−排斥优化算法；极端梯度提升（eXtreme Gradient Boosting，XGBoost）模型；沙普利加性解释（SHapley Additive exPlanations，SHAP）